Materials Transactions, Vol. 53, No. 11 (2012) pp. 1905 to 1909

Impact of Strain Rate on Thermomechanical Coupling Effects in TiNi SMA Subjected to Compression

Elzbieta A. Pieczyska[1], Hisaaki Tobushi[2], Karol Kulasinski[1] and Kohei Takeda[2]

[1]*Institute of Fundamental Technological Research, PAS, Pawinskiego 5B, 02-106 Warsaw, Poland*
[2]*Aichi Institute of Technology, Toyota 470-0392, Japan*

In this study, the thermomechanical coupling effects accompanying stress-induced martensitic transformation in TiNi shape memory alloy subjected to compression test were investigated. The mechanical characteristics were elaborated and the temperature changes related to the exothermic martensitic forward transformation and the endothermic reverse one were measured in a contactless manner by a fast and sensitive infrared camera. The obtained temperature changes of the specimen depend on the strain rate applied. At higher strain rate, greater temperature changes were observed, because the heat flow to the surroundings was lower and the process was closer to adiabatic conditions. The temperature changes of the shape memory alloy significantly influence its stress–strain characteristics. Moreover, the energy dissipated during a compression cycle was calculated for various strain rates. The study revealed that both the loading work and recoverable strain energy increase with increasing strain rate, while the dissipated energy fraction decreases. [doi:10.2320/matertrans.M2012212]

(Received June 11, 2012; Accepted August 16, 2012; Published October 11, 2012)

Keywords: *shape memory alloy, compression test, exothermic/endothermic transformation, infrared camera, energy dissipation*

1. Introduction

Shape-memory alloys (SMA), being very attractive materials, find recently more and more innovative applications and their interesting properties are investigated in a large number of research centres in many countries. In fact, SMA's behaviour strongly depends on temperature, which still needs to be thoroughly investigated due to the unsatisfactory number of such experimental results and publications, as well as to ever-increasing demands from industry. The thermomechanical coupling occurring in SMA during loading and unloading processes is a strong effect accompanying stress-induced martensitic transformation (SIMT). It is well known that the forward martensitic transformation is exothermic whilst the reverse one exhibits endothermic property. However, both processes are very complex and are strongly related to the microstructure evolution. Although the thermomechanical properties of SMA under various strain rates have been investigated by tension testing, e.g.,[1–9] there are not many results published related to torsion,[3,11] shear[2,10] or compression.[12–14]

In this paper, some results obtained for TiNi SMA under compression with various strain rates are presented. The goal was to examine the impact of strain rate on the thermomechanical coupling effects.

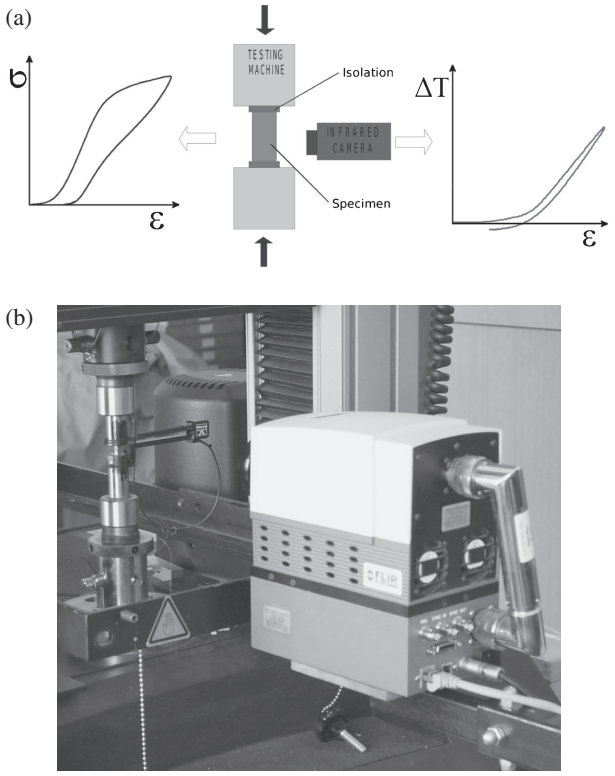

Fig. 1 Scheme (a) and photography (b) of the experimental setup.

2. Experimental Details

The TiNi SMA studied in this research has been produced by Furukawa Electric Co. Small rods of 5 mm diameters and 7.5 mm length were subjected to compression tests on Instron testing machine. Two plates of mica were placed between the specimens and the compressing grips of the testing machine in order to set up some thermal isolation. A mechanical extensometer was coupled to the grips of the testing machine, providing, besides strain measurement, the strain rate control (Fig. 1). During a preliminary test a laser extensometer was also used. The laser extensometer measures the specimen strain independently of the testing machine, therefore more precisely than the mechanical extensometer, providing useful information on the mechanical characteristics of tested materials. Moreover, infrared radiation (IR) was measured from the specimen surface during the deformation process using a modern infrared camera Phoenix, Flir Co. The high-performance camera delivers infrared images with 538 Hz frequency and estimates the temperature remotely with accuracy up to 0.025 K. The laser extensometer cannot be used during the tests with IR camera due to its use perturbing the infrared measurement. Before the investigation, the SMA specimen was covered with a very thin layer of black ink in

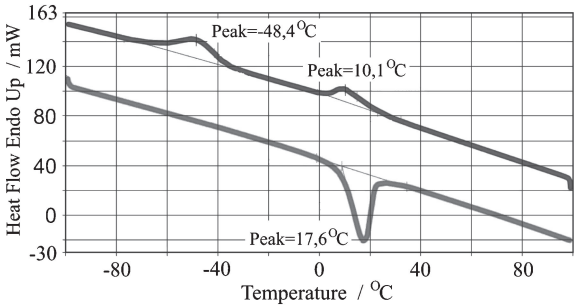

Fig. 2 DSC curves of a TiNi SMA sample obtained for two complete heating-cooling runs (courtesy of Danuta Stróż, University of Silesia).

order to make the surface more homogeneous with a higher, known coefficient of emissivity.

In order to investigate the characteristic transformation temperatures of the shape memory alloy, the differential scanning calorimetric (DSC) method has been applied. The DSC results obtained for the TiNi SMA are shown in Fig. 2. With respect to the DSC data, two peaks due to the R-phase transformation and the martensitic transformation are observed during cooling, and only one peak, due to the reverse transformation, is observed during heating. The reverse transformations, due to the R-phase transformation and the martensitic transformation, probably overlapped in this material, especially as some Ni_4Ti_3 precipitates were found during the microstructure investigations.[15] Moreover, the X-ray diffraction patterns obtained for the TiNi initial state prove presence of the B2 phase in the sample.

The SMA transformation temperatures estimated from Fig. 2 may be as follows: $M_s = -36°C$, $M_f = -67°C$, $A_s = 8°C$, $A_f = 23°C$, $R_s = 23°C$ and $R_f = 3°C$. R_s and R_f are the R-phase transformation start and finish temperatures. For the loading-unloading process carried out at room temperature (21.5°C) in vicinity of the A_f temperature, a mix of the superelasticity (SE) and shape memory effect (SME) can be expected. The residual strain recorded after the unloading can be removed by further heating the deformed specimens at a temperature above the austenite finish temperature A_f.

3. Mechanical and Temperature Characteristics Obtained for Various Strain Rates

The compression tests were carried out with various strain rates equal to 10^{-4}, 10^{-3}, 10^{-2}, 5×10^{-2} and $10^{-1}\,s^{-1}$. During the TiNi SMA loading and unloading the temperature distribution observed on the specimen surface was not uniform, we can therefore acknowledge that the transformation process occurs non-homogeneously. An example of the thermograms, i.e., the temperature distribution on the specimen surface obtained at the strain rate $10^{-1}\,s^{-1}$ during loading (a), (b) and unloading (c) are shown in Fig. 3. The points corresponding to the thermograms are marked on the stress–strain curve (Fig. 3(d)). In fact, when looking at the thermograms, we do not observe narrow, Luders-like, transformation bands that we have recorded during the TiNi tension tests.[4,5,9] Instead, the wide bands of higher temperature are visible, developing in the central area of the

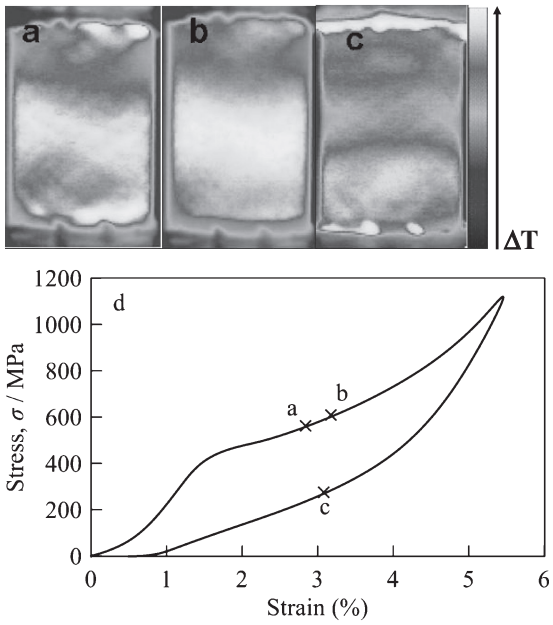

Fig. 3 Thermograms obtained by fast Phoenix infrared camera for the TiNi SMA specimen subjected to compression with strain rate $10^{-1}\,s^{-1}$ during: (a), (b) loading; (c) unloading. Stress–strain curve (d).

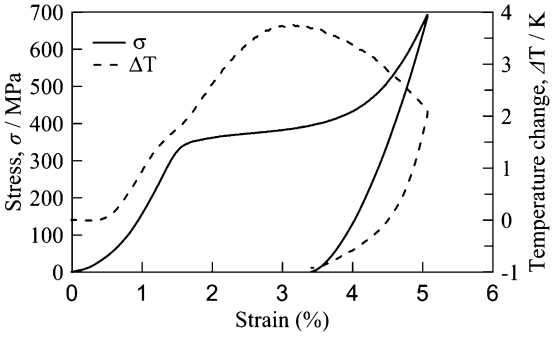

Fig. 4 Stress and temperature variation vs. strain curves obtained for TiNi SMA during compression with strain rate $10^{-3}\,s^{-1}$.

specimen (Figs. 3(a), 3(b)), and indicating the inhomogeneity of the forward transformation process. Similarly, a band of the lower temperature developing during the specimen unloading (Fig. 3(c)) exhibits the reverse transformation inhomogeneity.

In order to study the effect of strain rate on thermomechanical coupling in TiNi SMA, an average temperature was calculated from the specimen surface for all the strain rates applied. It enables us to compare the temperature changes of the specimens to the mechanical characteristics obtained during the SMA compression loading-unloading tests. The obtained stress and temperature evolution as a function of strain during compression with strain rates 10^{-3}, 10^{-2} and $10^{-1}\,s^{-1}$ are presented in Figs. 4–6, respectively.

The mechanical characteristics accompanied by the average temperature variation of the specimen obtained for strain rate $10^{-3}\,s^{-1}$ in Fig. 4 indicates that the SMA temperature starts raising at the strain of approximately 0.4%, manifesting the process of nucleation of exothermic forward transformation. Next, the temperature increases up to

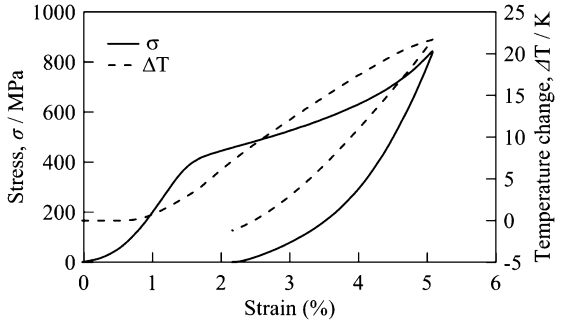

Fig. 5 Stress and temperature variation vs. strain curves obtained for TiNi SMA during compression with strain rate $10^{-2}\,s^{-1}$.

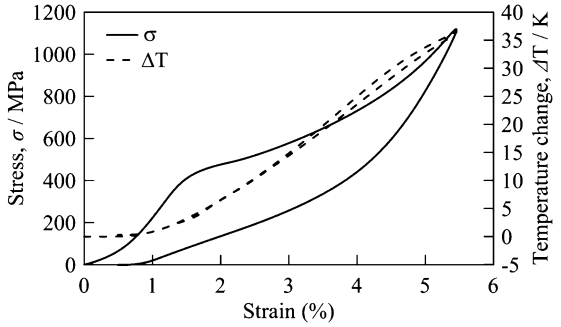

Fig. 6 Stress and temperature variation vs. strain curves obtained for TiNi SMA during compression with strain rate $10^{-1}\,s^{-1}$.

3.7 K at the strain of approximately 3.2%. At higher strains, a decrease in the specimen temperature is observed proving that the heat flow to the surroundings is greater than the heat production related to the exothermic martensitic forward transformation. This indicates that although the transformation is still in progress, it does not develop so fast from this loading stage, if the strain rate is slow. During the unloading process, much more significant temperature decrease related to elastic unloading followed by endothermic reverse transformation, is observed. After unloading was completed, a significant residual strain of 3.4% related to the shape memory effect was recorded (Fig. 4).

With respect to the nonlinearity of the stress–strain curves recorded at the beginning of the SMA compression loading, under a stress below 50 MPa and a strain less than 0.6%, no nonlinearity was recorded by the applied laser extensometer. It means that the nonlinearity is rather not caused by the *R*-phase, but results mainly from the machine-isolation-specimen backlash elimination.

At higher strain rate equal to $10^{-2}\,s^{-1}$, the temperature variation related to the phase transformation is much higher (up to 22 K) which significantly influences the mechanical characteristics (Fig. 5). Namely, the slope of the stress–strain curve during the loading is steeper and the residual strain recorded after the SMA unloading is much lower (2.2%), showing partial superelasticity. Moreover, the stress and temperature vs. strain profiles are different from those obtained for lower strain rate. Both the maximal temperature change of 22 K as well as the maximal stress (850 MPa) values have been obtained at the end of the loading, at the strain value of 5% (Fig. 5). The same tendency was observed at the strain rate $10^{-1}\,s^{-1}$.

The mechanical characteristics and the average specimen temperature results, obtained for the highest strain rate applied in this approach equal to $10^{-1}\,s^{-1}$, are shown in Fig. 6. The maximal temperature increase recorded for so high deformation rate exceeds 37 K, being accompanied by the stress increase up to 1100 MPa. The specimen is deformed almost superelasticaly — the residual strain recorded after the SMA unloading is only 0.6%, resulting in superelasticity. The hysteresis loop keeps narrowing and the temperature curves for loading and unloading overlap. Therefore, the measurement takes place in adiabatic conditions. After unloading, the specimen temperature returns to its initial value, while for lower strain rate it drops below the initial temperature (Figs. 4, 5).

At higher strain rates, the temperature variation related to the phase transformation process is much higher which influences significantly the stress–strain profile: the slope of the stress–strain curve during the loading is steeper and the residual strain recorded after the SMA unloading is lower.

Summarizing the results shown in Figs. 4–6, we can state that increasing the deformation rate results in the narrowing of the temperature and stress hysteresis and decreasing the value of residual stress after the SMA specimen unloading, and therefore changing the characteristics from the shape memory effect to the superelasticity.

4. Comparison of Thermomechanical Coupling Effects Occurring in TiNi SMA Subjected to Compression

The stress–strain characteristics obtained for TiNi SMA in compression at three various strain rates 10^{-3}, 10^{-2} and $10^{-1}\,s^{-1}$ shown in Figs. 4–6 are presented in one diagram in Fig. 7. In addition, a comparison of the temperature variation vs. stress curves obtained for these three strain rates is shown in one diagram in Fig. 8.

One can notice looking at Figs. 4–6 and Figs. 7, 8 that:

(1) no significant discrepancies are observed in the character of the stress–strain curves within the elastic strain range
(2) the higher the strain rate, the higher the specimen temperature which follows the higher stress of the SMA yielding related to the stress-induced phase transformation process
(3) the higher the strain rate, the higher the maximal stress observed at the end of the strain range applied
(4) the higher the strain rate, the smaller residual strain and the better shape recovery was recorded.

The SMA stress–strain behavior manifested at various strain rates can be explained in the following way. Both the forward and the reverse transformation stresses in SMA increase in proportion to the temperature. Therefore, in general, the shape memory effect is observed at low temperature (below M_s), the partial superelasticity at higher temperature and the perfect superelasticity above A_f temperature. It is also well known that the residual strain recorded after SMA unloading can be removed during the further alloy heating at the temperature above A_f. During the compression carried out at high strain rates, the SMA specimen attained high temperature due to the exothermic transformation and the test was close to adiabatic conditions.

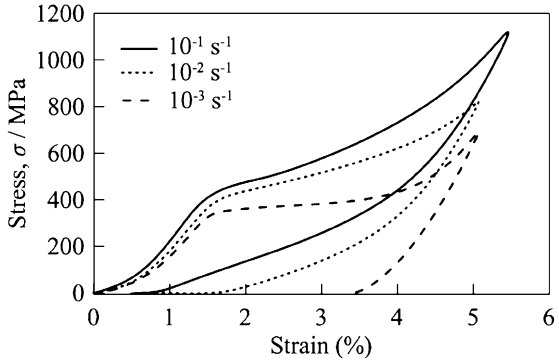

Fig. 7 Comparison of stress vs. strain curves obtained for TiNi SMA during compression with various strain rates: 10^{-1}, 10^{-2} and $10^{-1}\,s^{-1}$.

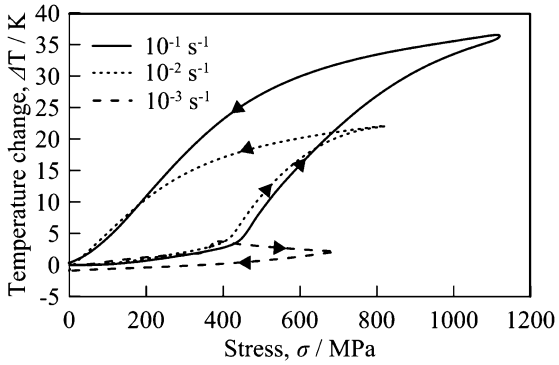

Fig. 8 Comparison of temperature variation vs. stress curves obtained for TiNi SMA during compression with various strain rates: 10^{-1}, 10^{-2} and $10^{-1}\,s^{-1}$.

Table 1 Characteristic values obtained during TiNi SMA compression for various strain rates.

Strain rate	$10^{-3}\,s^{-1}$	$10^{-2}\,s^{-1}$	$10^{-1}\,s^{-1}$
Stress of SIMT yield start	360 MPa	415 MPa	430 MPa
Maximal stress	700 MPa	860 MPa	1140 MPa
Max. average temp. increase	3.7 K	22 K	37 K
Residual strain after unloading	3.4%	2.1%	0.6%

If the strain rate is high, the temperature rise is large, resulting in an increase in the reverse transformation stress. The reverse transformation behavior is affected by the temperature rise that occurs during the forward transformation. The dependence of the deformation behavior on temperature must appear in the compression test depending on the temperature rise due to the dependence on strain rate. In this way at the strain rate of $10^{-1}\,s^{-1}$ the hysteresis loop is narrow and an almost total shape recovery is observed, resulting in superelasticity.

A comparison of some mechanical and temperature results obtained during the SMA compression carried out with strain rates 10^{-3}, 10^{-2}, $10^{-1}\,s^{-1}$ and presented in Figs. 7, 8 is shown in Table 1.

Looking at Figs. 7 and 8 and the data shown in Table 1 it can be summarized that similarly to the tension, the temperature variation related to the compression-induced phase transformation is much greater at higher strain rates, influencing significantly the stress–strain profile. Namely, the slope of the stress–strain curve obtained during the SMA loading is steeper, the achieved maximal stress value is higher and the residual strain recorded after the unloading is lower.

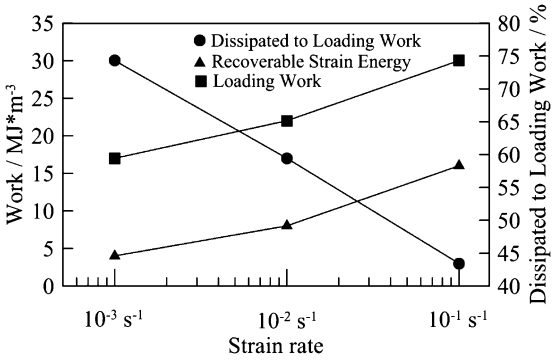

Fig. 9 Loading work, recoverable strain energy and dissipated to loading work in TiNi tested with various strain rates; $\varepsilon_{max} = 5\%$.

5. Dissipated Work and Recoverable Strain Energy

A dissipated energy study for various temperature conditions has been estimated for TiNi SMA subjected to tension test and presented in Ref. 16). Here we present loading and unloading work data, as well as the dissipated energy in TiNi SMA specimens subjected to compression test carried out with various strain rates. The obtained results are presented in Figs. 9, 10 and Table 2.

Loading work (W_L) and unloading work (W_U) can be calculated per unit volume as follows:

$$W_L = \int_A^B \sigma \cdot d\varepsilon \tag{1}$$

$$W_U = \int_B^C \sigma \cdot d\varepsilon \tag{2}$$

where A denotes the beginning of loading, B is end of loading and C is end of unloading; σ and ε are the stress and strain, respectively. W_U denotes the recoverable strain energy per unit volume.

Then, the dissipated energy, W_D, can be represented as:

$$W_D \equiv W_L - W_U > 0 \tag{3}$$

$$D = \frac{W_D}{W_L} = \frac{W_L - W_U}{W_L} = 1 - \frac{W_U}{W_L} = 1 - \frac{\int_B^C \sigma \cdot d\varepsilon}{\int_A^B \sigma \cdot d\varepsilon} \tag{4}$$

The ratio D tells what share of the loading work is dissipated, mainly turned into heat. The loading, unloading work and dissipated energy values for various strain rates are shown in Table 2 and in Fig. 9 in logarithmic scale. As we can observe, there is a strong correlation between the ratio of dissipated energy to loading work D and the strain rate. The decrease of D is close to exponential along the strain rate.

Besides that, a regular and monotonic increase of both loading work and recoverable strain energy can be observed along the strain rate (Figs. 9, 10). It means that the faster the SMA specimen is deformed, the greater work it does, because the greater is the mechanical resistance of the material. The

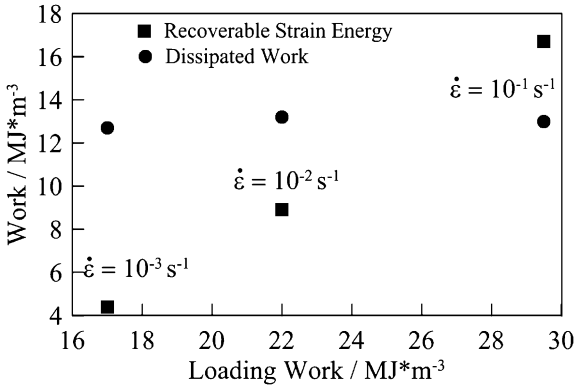

Fig. 10 Strain energy and dissipated work vs. loading work in TiNi SMA tested with various strain rates; $\varepsilon_{max} = 5\%$.

Table 2 Loading work, recoverable strain energy and dissipated energy for various strain rates; $\varepsilon_{max} = 5\%$.

Strain rate, s^{-1}	Loading work, MJ/m^3	Recoverable strain energy, MJ/m^3	Dissipated energy, MJ/m^3	Dissipated energy/ Loading work, $MJ/m^3/MJ/m^3$
10^{-1}	29.57	16.64	12.93	43.7%
10^{-2}	22.05	8.86	13.19	59.8%
10^{-3}	16.99	4.37	12.62	74.3%

recoverable strain energy and dissipated work vs. loading work in TiNi SMA tested for various strain rates are shown in Fig. 10. One can observe that there is a strong, almost linear correlation between the loading work and recoverable strain energy. Moreover, an interesting fact is that the dissipated work does not vary significantly with the loading work; we can therefore state that it is constant.

Loading work, recoverable strain energy and dissipated work obtained for various strain rates are presented in Table 2. One can notice that both the loading and recoverable strain energy increase with the strain rate. A similar tendency may be noticed regarding dissipated energy to loading work ratio.

The ratio D decrease with increasing strain rate (Fig. 9) may seem contrary to the temperature change increase. However, the observed results are caused by a very strong thermomechanical coupling effects, occurring in shape memory alloys and significant contribution of so called "latent heat" of phase transformation. Despite growing loading work and strain energy values, the dissipated energy does not change importantly (Table 2). Moreover, we are aware that regardless of the strain rate, comparative amount of heat is probably produced due to the SMA loading and the stress-induced martensitic transformation process. However, the time can differ of several orders of magnitude, causing huge discrepancies on the SMA specimen temperature, obtained for various strain rates.

6. Conclusions

This study shows significant differences between the effects of thermomechanical couplings, experimentally estimated for TiNi shape memory alloy subjected to compression with various strain rates. The differences are caused by the latent heat that accompanies the stress-induced martensitic transformation process, causing an increase in the specimen temperature, followed by the increase of stress. At low strain rate, the heat flows to the specimen grips and surroundings. At the higher strain rates the process is closer to adiabatic conditions and the higher increase of the specimen temperature is recorded. The higher temperature increase causes the higher stress during the SMA loading and the higher shape recovery after the unloading, resulting in superelasticity.

Moreover, the energy dissipated and recoverable strain energy during the compression cycle were calculated for various strain rates. The study revealed that both the loading work and recoverable strain energy increase with augmenting strain rate, while the dissipated energy to loading work fraction decreases. Nonetheless, the absolute values of the dissipated energy remain comparatively constant.

Acknowledgments

The authors acknowledge the Polish Ministry of Science and Higher Education; Grant 501220837, the National Center of Science: Grant 2011/01/M/ST8/07754 and the Japan Society for the Promotion of Science: Grant 23560103. Assistance of Dr J. Luckner in obtaining some experimental data is appreciated. The infrared measurement was carried out by Dr M. Maj to whom the authors wish to express their gratitude. Correction of the text by Will Hardwick is gratefully acknowledged.

REFERENCES

1) J. A. Shaw and S. Kyriakides: Acta Mater. **45** (1997) 683–700.
2) S. P. Gadaj, W. K. Nowacki and E. A. Pieczyska: Infrared Phys. Technol. **43** (2002) 151–155.
3) Q. P. Sun and Z. Q. Li: Int. J. Solids Struct. **39** (2002) 3797–3809.
4) E. A. Pieczyska, S. P. Gadaj, W. K. Nowacki and H. Tobushi: Mater. Trans. **47** (2006) 670–676.
5) E. A. Pieczyska, S. P. Gadaj, W. K. Nowacki and H. Tobushi: Exp. Mech. **46** (2006) 531–542.
6) D. Favier, H. Louche, P. Schlosser, L. Orgeas, P. Vacher and L. Debove: Acta Mater. **55** (2007) 5310–5322.
7) E. A. Pieczyska, H. Tobushi, W. K. Nowacki, S. P. Gadaj and T. Sakuragi: Mater. Trans. **48** (2007) 2679–2686.
8) X. Zhang, P. Feng, Y. He, T. Yu and Q. P. Sun: Int. J. Mech. Sci. **52** (2010) 1660–1670.
9) E. A. Pieczyska: J. Mod. Opt. **57** (2010) 1700–1707.
10) E. A. Pieczyska, S. P. Gadaj, W. K. Nowacki, J. Luckner and H. Tobushi: Strain **45** (2009) 93–100.
11) H. Tobushi, E. A. Pieczyska, W. K. Nowacki, T. Sakuragi and Y. Sugimoto: Arch. Mech. **61** (2009) 241–257.
12) J. M. Dutkiewicz, W. Maziarz, T. Czeppe, L. Lityńska, W. K. Nowacki, S. P. Gadaj, J. Luckner and E. A. Pieczyska: Eur. Phys. J. **158** (2008) 59–65.
13) E. A. Pieczyska, J. Dutkiewicz, F. Masdeu, J. Luckner and R. Maciak: Arch. Metall. Mater. **56** (2011) 401–408.
14) P. C. C. Monteiro, Jr., M. A. Savi and T. A. Netto: J. Intell. Mater. Syst. Struct. **20** (2009) 1675–1687.
15) K. Yamauchi, I. Ohkata, K. Tsuchiya and S. Miyazaki (eds.): *Shape Memory and Superelastic Alloys*, (Woodhead Publishing Limited, 2011).
16) E. A. Pieczyska, S. P. Gadaj, W. K. Nowacki, K. Hoshio, Y. Makino and H. Tobushi: Sci. Tech. Adv. Mater. **6** (2005) 889–894.